



Cite this: *Phys. Chem. Chem. Phys.*, 2024, 26, 15902

# O<sub>2</sub> activation by subnanometer Re–Pt clusters supported on TiO<sub>2</sub>(110): exploring adsorption sites†

Andrés Álvarez-García,<sup>a</sup> Luis M. Molina<sup>b</sup> and Ignacio L. Garzón<sup>ib</sup>\*<sup>a</sup>

Activation of O<sub>2</sub> by subnanometer metal clusters is a fundamental step in the reactivity and oxidation processes of single-cluster catalysts. In this work, we examine the adsorption and dissociation of O<sub>2</sub> on Re<sub>n</sub>Pt<sub>m</sub> ( $n + m = 5$ ) clusters supported on rutile TiO<sub>2</sub>(110) using DFT calculations. The adhesion energies of Re<sub>n</sub>Pt<sub>m</sub> clusters on the support are high, indicating significant stability of the supported clusters. Furthermore, the bimetallic Re–Pt clusters attach to the surface through the Re atoms. The oxygen molecule was adsorbed on three sites of the supported systems: the metal cluster, the surface, and the interface. At the metal cluster site, the O<sub>2</sub> molecule binds strongly to Re<sub>n</sub>Pt<sub>m</sub> clusters, especially on the Re-rich clusters. O<sub>2</sub> activation occurs by charge transfer from the metal atoms to the molecule. The dissociation of O<sub>2</sub> on the Re<sub>n</sub>Pt<sub>m</sub> clusters is an exothermic process with low barriers. As a result, subnanometer Re–Pt clusters can be susceptible to oxidation. Similar results are obtained at the metal-support interface, where both the surface and cluster transfer charge to O<sub>2</sub>. To surface sites, molecular oxygen is adsorbed onto the Ti<sub>5c</sub> atoms with moderate adsorption energies. The polarons, which are produced by the interaction between the metal cluster and the surface, participate in the activation of the molecule. However, dissociating O<sub>2</sub> in these sites is challenging due to the endothermic nature of the process and the high energy barriers involved. Our findings provide novel insights into the reactivity of supported clusters, specifically regarding the O<sub>2</sub> activation by Re–Pt clusters on rutile TiO<sub>2</sub>(110).

Received 14th March 2024,  
Accepted 15th May 2024

DOI: 10.1039/d4cp01118j

rs.li/pccp

## 1 Introduction

Supported metal clusters (SMCs) represent a category of heterogeneous catalysts comprising metal clusters attached to solid supports, such as metal oxides.<sup>1</sup> Re–Pt clusters supported on titania are employed as catalysts for the water–gas shift reaction<sup>2</sup> and CO oxidation.<sup>3,4</sup> Rhenium has a variety of valence states and higher oxophilicity than other noble metals (Pt, Ir), which may enhance catalytic multifunctionality.<sup>5</sup> The utilization of Re–Pt catalysts leads to an economical process because

of their extended catalyst lifespan and high yield of desired products.<sup>6</sup> The bimetallic system of Re–Pt exhibits unique properties that differ from those of pure Pt and pure Re in catalytic reactions.<sup>3</sup> The catalyst containing Re–Pt/TiO<sub>2</sub> exhibits higher activity than the pure Pt/TiO<sub>2</sub> catalyst for the water gas shift (WGS) reaction.<sup>7</sup> The interaction between oxygen and Re–Pt bimetallic clusters is relevant in the aforementioned reactions because PtO<sub>x</sub> and ReO<sub>x</sub> can act as promoters or inhibitors.<sup>8</sup> The activation of O<sub>2</sub> is a pivotal step in oxidation processes, resulting in the creation of more reactive species, such as superoxo, peroxy, and atomic oxygen.<sup>9,10</sup> Several factors can influence the activation of O<sub>2</sub>, including the support type, cluster size, and interface perimeter.<sup>11–13</sup> Additionally, metals featuring a low O<sub>2</sub> dissociation barrier exhibit a tendency to adsorb O<sub>2</sub> and O strongly, rendering them susceptible to oxidation.<sup>14</sup>

Recently, there has been an increasing interest in subnanometer clusters as single-cluster catalysts (SCCs). Small metal clusters, typically composed of fewer than 20 atoms (with a diameter of less than 1 nm), are supported on suitable matrices to form SCCs.<sup>15</sup> They are an intermediate size between traditional metal nanoparticles and single-atom catalysts (SACs).<sup>16–18</sup> Subnanometer metal clusters exhibit unique physicochemical

<sup>a</sup> Instituto de Física, Universidad Nacional Autónoma de México, Apartado Postal 20-364, Ciudad de México 01000, Mexico. E-mail: garzon@fisica.unam.mx

<sup>b</sup> Departamento de Física Teórica, Atómica y Óptica, Universidad de Valladolid, E-47011 Valladolid, Spain

† Electronic supplementary information (ESI) available: Table S1 presents the Bader charge analysis of supported Re<sub>n</sub>Pt<sub>m</sub> clusters on TiO<sub>2</sub>(110), while Table S3 displays this analysis for O<sub>2</sub> activation on the supported clusters. Table S2 shows the structural and energetic parameters for O<sub>2</sub> adsorption on the surface site in the presence of supported Re<sub>n</sub>Pt<sub>m</sub> clusters. The most stable structures of gas-phase clusters are displayed in Fig. S1. The lowest energy isomers are displayed in Fig. S2 and S3. The most stable structures for O<sub>2</sub> dissociation on Re<sub>n</sub>Pt<sub>m</sub> supported clusters are shown in Fig. S4. Finally, the structures for dissociative adsorption of O<sub>2</sub> on the Re–Ti interface are presented in Fig. S5. See DOI: <https://doi.org/10.1039/d4cp01118j>



properties due to quantum confinement effects.<sup>19</sup> Controlling the size and arrangement of SCCs with atomic precision is crucial for adjusting the activity and stability of clusters in different catalytic applications.<sup>20</sup> Furthermore, the precise control of subnanometer clusters can result in the formation of bimetallic catalysts, such as Au<sub>4</sub>Pt<sub>2</sub><sup>21</sup> and Rh<sub>1</sub>Co<sub>3</sub><sup>22</sup> clusters.

The stability of subnanometer clusters is maintained by the metal-support interactions, as well as the low kinetic energy deposition.<sup>23</sup> Interactions between highly reactive metals (with incomplete d-shells), such as Re, and reducible oxides, such as titania, can stabilize supported metal clusters composed of only a few atoms.<sup>24–26</sup> Ultra-small Re clusters (size = 2–13 atoms) were deposited on graphene and studied by high annular dark-field scanning transmission electron microscopy (HAADF-STEM), where Re clusters presented 3D structures above four-atom size.<sup>27</sup> Subnanometer Pt<sub>*n*</sub> (*n* = 4, 7–10, 15) clusters were deposited on the TiO<sub>2</sub>(110) surface and imaged at atomic resolution using an ultrahigh vacuum scanning tunneling microscope.<sup>28</sup> The Pt<sub>7</sub> cluster on TiO<sub>2</sub>(110) exhibits catalytic activity in CO oxidation, where reduction conditions can play a significant role in CO<sub>2</sub> production.<sup>29</sup> While there are no reports of subnanometer-scale Re–Pt clusters, they have been studied in larger clusters.<sup>7</sup> In our previous work, we analyzed the structure of Re–Pt clusters in both the gas phase and supported on the MgO(100) surface. Our findings revealed a transition from a 2D to a 3D configuration at size five.<sup>30</sup> In addition, five-atom size clusters allow for the exploration of 3D configurations, with atoms directly interacting with the substrate and others forming a second layer.

The Cu<sub>5</sub> cluster has been synthesized with atomic precision and exhibits stability to ultraviolet radiation, temperature, and pH, rendering it an ideal model for the study of polarons in oxide-supported clusters.<sup>31</sup> Oxides can serve as inert matrices for dispersing metal nanoparticles or as catalysts themselves. The reducible oxides, such as TiO<sub>2</sub>, CeO<sub>2</sub>, and Fe<sub>2</sub>O<sub>3</sub>, are capable of exchanging oxygen atoms, making them effective in oxidation reactions.<sup>32–34</sup> In particular, the reactivity of rutile TiO<sub>2</sub>(110) surface for O<sub>2</sub> adsorption and dissociation has been studied.<sup>35</sup> Oxygen vacancies (O<sub>v</sub>) on the TiO<sub>2</sub>(110) surface act as a source of excess electrons, leading to the dissociation of O<sub>2</sub>.<sup>36,37</sup> This excess of electrons can also be achieved by charge transfer from metal clusters with low resistance to electron donation.<sup>38–40</sup> Specifically, Cu<sub>5</sub> and Ag<sub>5</sub> clusters donate electrons to the support, inducing the formation of one or two polarons.<sup>41–43</sup> The excess charge is located in the 3d states of Ti, which causes a reduction of its oxidation state from Ti<sup>4+</sup> to Ti<sup>3+</sup>. Therefore, the study of subnanometer clusters of five-atom size supported on titania is of significant interest due to their computational simplicity, preference for 3D conformations, and the existing background on this topic.

Modeling subnanometer clusters supported on metal oxides is challenging due to their structural intricacies.<sup>44</sup> To address this issue, utilizing global optimization algorithms such as Basin-Hopping<sup>45</sup> or Genetic Algorithms<sup>46</sup> in conjunction with Density Functional Theory (DFT) may be advantageous. In this manuscript, we present an extensive study of the structure of subnanometer Re<sub>*n*</sub>Pt<sub>*m*</sub> (*n* + *m* = 5) clusters supported on the

rutile TiO<sub>2</sub>(110) surface, evaluating the O<sub>2</sub> adsorption and activation on these bimetallic clusters as a function of their relative Re–Pt content. The configuration space of the supported clusters is explored using the Basin-Hopping DFT algorithm. Then, the most stable isomers were selected for a complete study of O<sub>2</sub> adsorption at all the possible binding sites: the metal cluster, the TiO<sub>2</sub>(110) surface away from the supported cluster, and the interfacial region around the cluster. The O–O bond activation is evaluated by various structural (bond length, O–O stretching frequency) and electronic parameters (spin magnetic moment, Bader charges, and density of states). Finally, the dissociation of O<sub>2</sub> is also studied using the Nudged Elastic Band (NEB) approach to obtain the activation barriers for this process.

## 2 Computational details

The structures of the gas-phase Pt<sub>*n*</sub>Re<sub>*m*</sub> (*n* + *m* = 5) clusters were obtained from our previous study,<sup>30</sup> where we performed a global optimization using the Basin-Hopping DFT (BH-DFT) algorithm coupled to VASP (ESI<sup>+</sup>). The TiO<sub>2</sub>(110) surface was constructed using a 4 × 2 slab with four trilayers, with the two bottom trilayers fixed to their positions in the bulk during relaxations. The vacuum in the *z*-direction was 20 Å, and the neighboring images in the horizontal direction were separated by at least 8 Å. A dipole correction perpendicular to the supercell is applied to the total energy. The search for the most stable structures of Pt<sub>*n*</sub>Re<sub>*m*</sub> (*n* + *m* = 5) clusters supported on TiO<sub>2</sub>(110) was performed using the BH-DFT algorithm with 50 Monte Carlo steps.

DFT calculations were performed in the VASP code<sup>47</sup> employing the PBE functional<sup>48</sup> and the projector augmented wave (PAW) potentials.<sup>49,50</sup> The cutoff energy for the plane-wave basis set was 400 eV. Ti(3s, 3p, 3d, 4s), O(2s, 2p), Pt(5d, 6s), and Re(5d, 6s) electrons were treated explicitly as valence. For titanium, the DFT+U formalism<sup>51</sup> was used to describe the highly localized d-electrons,<sup>52</sup> with the parameter for the Ti(3d) level set to 4.5 eV. The evaluation of the reducibility of the surface was performed by analyzing the spin magnetic moment and spin density of the system atoms. The convergence criteria of the electronic energy of the self-consistent field (SCF) and the forces of the geometric relaxations were 10<sup>−6</sup> eV and 0.01 eV Å<sup>−1</sup>, respectively. A single  $\Gamma$  point was used for integration of the Brillouin zone, since the large size of the unit cell already results in converged binding energies including only this single point in the calculations.

The adsorption energy for Re<sub>*n*</sub>Pt<sub>*m*</sub> clusters ( $E_{\text{ads}}[\text{cluster}]$ ) supported on TiO<sub>2</sub>(110) was calculated as<sup>53</sup>

$$E_{\text{ads}}[\text{cluster}] = -E[\text{Re}_n\text{Pt}_m/\text{TiO}_2] + E[\text{TiO}_2] + E[\text{Re}_n\text{Pt}_m]$$

where  $E[\text{Re}_n\text{Pt}_m/\text{TiO}_2]$ ,  $E[\text{Re}_n\text{Pt}_m]$ , and  $E[\text{TiO}_2]$  correspond to the total energy of the putative global minimum of the supported clusters, gas-phase clusters, and the relaxed TiO<sub>2</sub>(110) surface, respectively. The adhesion energy ( $E_{\text{adh}}$ ) was calculated using a similar equation, but the energies of the gas-phase clusters and the surface were taken at a fixed geometry of the supported cluster.



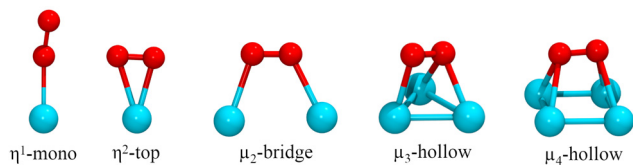


Fig. 1 Modes of adsorption of  $O_2$  on  $Re_nPt_m$  clusters.

The adsorption of the  $O_2$  molecule on the clusters was studied on several binding configurations, depicted in Fig. 1. The adsorption mode  $\eta^1$  is the bonding of an O atom to a metal atom. In the  $\eta^2$ , the metal is bonded to the two atoms of the oxygen molecule. The other sites involve  $O_2$  bonding on multiple metal atoms ( $\mu_2$ ,  $\mu_3$ ,  $\mu_4$ ). Previous studies have evaluated these types of adsorption sites for oxygen molecule on metal clusters.<sup>54,55</sup> On each case, before each structural optimization, the  $O_2$  molecule was positioned initially 2.2 Å away from the binding site.

The adsorption energy for  $O_2$  to the cluster, either supported or in the gas phase, ( $E_{\text{ads}}[O_2]$ ) was calculated as

$$E_{\text{ads}}[O_2] = -E_{O_2/\text{cluster}} + E_{O_2} + E_{\text{cluster}}$$

where  $E_{O_2/\text{cluster}}$ ,  $E_{O_2}$ , and  $E_{\text{cluster}}$  are the energies for the complex  $O_2$ -cluster,  $O_2$  molecule in the gas-phase, and cluster, respectively. The cluster energy applies to the gas-phase or supported cluster on the  $TiO_2(110)$  surface.

The charge transfer was studied through a charge density analysis with the Bader approach.<sup>56,57</sup> The projected of Density of States (PDOS) over each atom of the system was calculated using VASPKIT code<sup>58</sup> with a Gaussian broadening equal to 0.1 eV. The climbing image Nudge-elastic-band (CI-NEB) method was employed to determine the transition states for the reaction pathways of the  $O_2$  dissociation reaction.<sup>59</sup> Each transition state (TS) presented only one imaginary frequency, which verifies that it is a maximum in the potential energy surface (PES). The stretching frequency of the oxygen molecule was calculated using the harmonic finite difference approximation.<sup>60,61</sup> We also studied how temperature affects the oxygen dissociation reaction in gas-phase clusters. We used the harmonic finite difference approximation to calculate the vibrations of the reactants ( $O_2$  adsorption on the clusters) and the products ( $O_2$  dissociation). The free energy at 300 K and 1 atm was determined using the post-processing code VASPKIT,<sup>58</sup> considering rotational, vibrational, translational, and electronic contributions.

## 3 Results

### 3.1 Structure and stability of $Re_nPt_m$ ( $n + m = 5$ ) clusters supported on the $TiO_2(110)$

The  $TiO_2(110)$  surface has three types of sites in its topmost layer: the two-coordinate protruding oxygen ( $O_{2c}$ ), the three-coordinate oxygen ( $O_{3c}$ ), and the five-coordinate titanium ( $Ti_{5c}$ ). The  $O_{2c}$  atoms protrude in one dimensional rows above the plane where  $Ti_{5c}$  and  $O_{3c}$  sites are located. A global optimization of  $Re_nPt_m$  ( $n + m = 5$ ) clusters supported on  $TiO_2(110)$  was

performed using Basin-Hopping DFT. Fig. 2 shows the structure, absorption and adhesion energies of the global minima for each of the  $Re_nPt_m/TiO_2(110)$  clusters. Although the calculations were performed with four trilayers (12 atomic layers), to improve visualization of the structure only the first trilayer of the surface is displayed. This slab model has been employed in prior investigations studying metal clusters of comparable size.<sup>62,63</sup>

All the clusters, excepting  $Re_1Pt_4$ , have a distorted square pyramidal shape, with its base in contact with the surface. At the global minima found, the clusters try to maximize the number of bonds between the metallic atoms in the bottom layer and the more reactive  $O_{2c}$  surface sites. In order to form stronger O-metal bonds by shortening the bond distance, the surface  $O_{2c}$  atoms suffer important lateral distortions of around 0.3–0.4 Å. The  $Re_1Pt_4$  cluster has a very different shape, more planar, and with only three atoms in direct contact with the surface. In the case of  $Pt_5$ , our results agree with the simulations performed by Jian *et al.*,<sup>64</sup> who obtained the putative global minima for  $Pt_n$  ( $n = 4-8$ ) on the rutile  $TiO_2(110)$  surface, with the  $Pt_5$  cluster also having a pyramidal square conformation.

In our previous work,<sup>30</sup> gas-phase  $Re_nPt_m$  ( $n + m = 5$ ) clusters were optimized using a similar Basin-Hopping DFT algorithm (ESI,† Fig. S1).  $Re_3Pt_2$ ,  $Re_2Pt_3$ , and  $Pt_5$  clusters have planar structures, while  $Re_5$ ,  $Re_4Pt_1$ , and  $Re_1Pt_4$  clusters presented three-dimensional structures. In particular, the  $Re_5$  cluster has a square pyramidal configuration, which does not change significantly after adsorption on the  $TiO_2(110)$  surface. The high internal binding energy of the  $Re_5$  cluster is the reason for this behavior, indicating a very strong metal-metal bond.

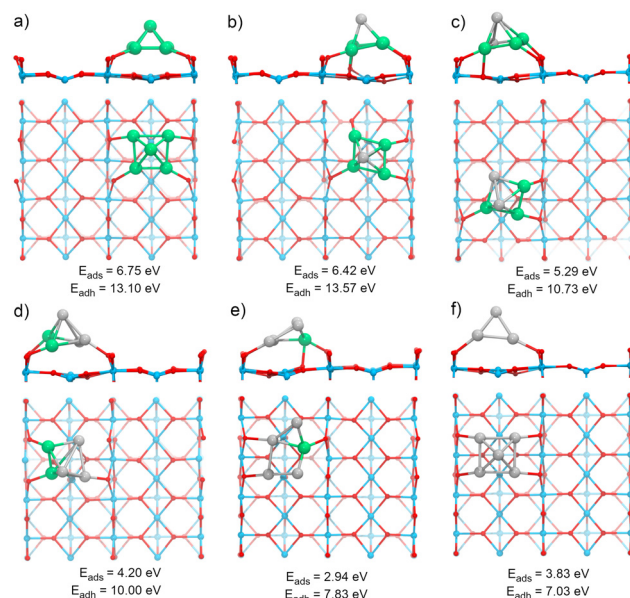


Fig. 2 Structure of  $Re_nPt_m$  ( $n + m = 5$ ) clusters supported on  $TiO_2(110)$  (Side and top views are displayed). (a)  $Re_5$ , (b)  $Re_4Pt_1$ , (c)  $Re_3Pt_2$ , (d)  $Re_2Pt_3$ , (e)  $Re_1Pt_4$ , (f)  $Pt_5$ . The adsorption ( $E_{\text{ads}}$ ) and adhesion ( $E_{\text{adh}}$ ) energies are displayed beneath each structure in eV. The side view only displays the final layer of the slab to aid the analysis. The colors green, gray, blue, and red represent the atoms Re, Pt, Ti, and O, respectively.



The rest of the clusters, are more fluxional, and the interaction with the substrate results in very important structural changes. For instance, the Pt<sub>5</sub> cluster changes from a planar house-shaped configuration to a square pyramid, which was similarly found on the ZrO<sub>2</sub>(101) surface.<sup>65</sup> In the ESI† (Fig. S2 and S3) we compare the global minimum found for each composition, with the first and second isomers (ISO1 and ISO2). For the clusters with a high content of Re, there are no competing isomers with the square pyramidal shape. However, as the Pt content increases, other alternate conformations have similar stabilities to the global minimum shape, as for example the ISO1 conformations for Pt<sub>3</sub>Re<sub>2</sub> and Pt<sub>4</sub>Re<sub>1</sub>, less than 0.1 eV apart from the GM one.

Several energetic parameters have been calculated to account for the cluster–surface interaction (Fig. 2). The adsorption energy of the clusters ( $E_{\text{ads}}[\text{cluster}]$ ) provides information about the stability of the cluster deposition on the substrate. In general,  $E_{\text{ads}}[\text{cluster}]$  decreases with an increasing amount of Pt in the cluster, with Re<sub>1</sub>Pt<sub>4</sub> being an exception which can be attributed to the high energetic cost of the cluster distortion that takes place during adsorption; indeed, the value of the adhesion energy for this cluster is actually larger than the one for pure Pt<sub>5</sub>,

The adhesion energy ( $E_{\text{adh}}$ ), which represents the strength of the interaction between the cluster and the surface, also decreases steadily with a increasing content of Pt. In all cases, the values for  $E_{\text{adh}}$  exceed 7 eV (and reach even 13 eV for Re-rich clusters), indicating a high stability of the supported clusters. The relaxed geometries show a marked tendency towards maximizing the number of bonds between Re atoms and surface oxygen atoms; for mixed clusters, Re atoms are always in contact with the substrate, and alternate conformations with Re atoms losing contact with the support are much less stable, as Fig. S2 and S3 (ESI†) show. Comparing the values of  $E_{\text{ads}}$  or  $E_{\text{adh}}$  for Re<sub>5</sub> and Pt<sub>5</sub> (which both share the same geometric arrangement) it is clear that the intrinsic strength of O–Re bonds is approximately twice as large as the one of O–Pt bonds. The cluster–surface interaction energies for other five atom clusters supported on TiO<sub>2</sub>(110) reported in the literature are 4.50, 4.53, 5.37, and 6.87 eV for the Cu<sub>5</sub>,<sup>38</sup> Ag<sub>5</sub>,<sup>42</sup> Au<sub>5</sub>,<sup>66</sup> and Pd<sub>5</sub><sup>66</sup> clusters, respectively. Thus, Re<sub>*n*</sub>Pt<sub>*m*</sub> (*n* + *m* = 5) clusters exhibit a higher affinity for the TiO<sub>2</sub>(110) surface compared to other clusters of the same size that have been previously reported. Interestingly, the formation of strong bonds between Re and the surface O atoms is affected by the reducible character of the TiO<sub>2</sub> oxide; the situation changes for a non-reducible oxide as MgO, where Re-rich clusters do not fit well on the support.<sup>30</sup>

The Bader charge analysis shows that the Re<sub>5</sub> cluster donates 2.04 electrons to the surface, while Pt<sub>5</sub> transfers only 0.25 electrons (see data in Fig. 3). For bimetallic clusters, the charge transfer to the substrate increases steadily with the Re composition (from 0.70 to 1.74 electrons). Therefore, the stronger interaction between Re and O atoms also results in a larger degree of charge transfer towards the surface. This charge is highly localized on the Ti atoms at the surface, as evidenced by the analysis of the spin magnetic moment. In Fig. 3, we have

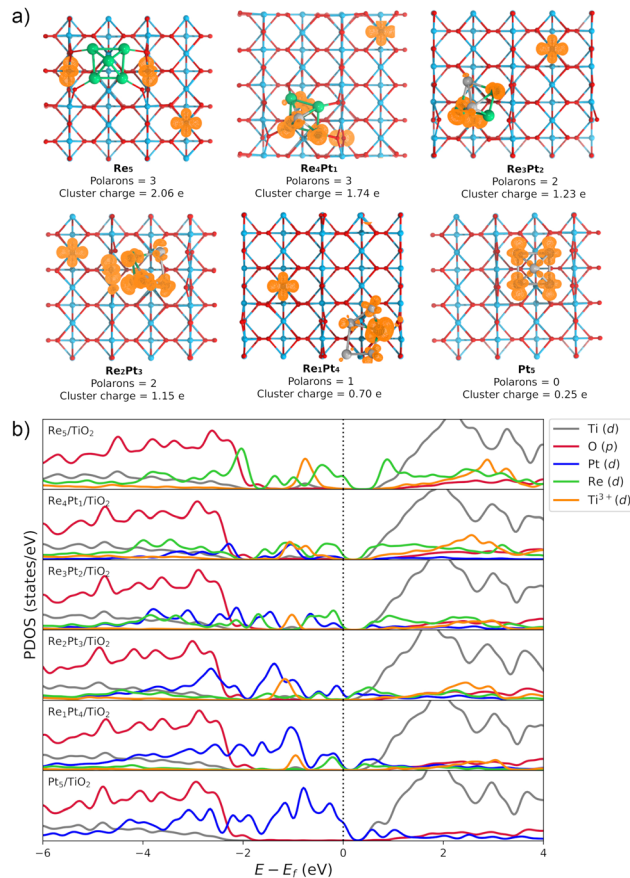


Fig. 3 Electronic properties of Re<sub>*n*</sub>Pt<sub>*m*</sub> (*n* + *m* = 5) clusters supported on TiO<sub>2</sub>(110). (a) The spin density for the supported clusters. The number of polarons formed and the charge transfer from the cluster to the substrate are displayed below each structure. The spin density isosurface is shown in orange. (b) The projected density of states (PDOS) for Re<sub>*n*</sub>Pt<sub>*m*</sub> (*n* + *m* = 5)/TiO<sub>2</sub>(110) clusters, where the cluster (Pt, Re) and polaron states (Ti<sup>3+</sup>) have been multiplied by six to ease the observation. The Gaussian broadening used in the projection is 0.10 eV.

calculated the spin density distribution and polaron formation for the supported clusters. The charge donation from clusters which contain Re results in polarons appearing on Ti<sup>3+</sup> sites. In the case of the Pt<sub>5</sub> cluster, the spin density is localized on the metal atoms, so no polarons are formed. In contrast, for the other clusters the spin density and spin magnetic moment are localized on the surface Ti atoms. The polarons are located below or to one side of the cluster. We find that the reducibility of the TiO<sub>2</sub>(110) surface and the number of polarons formed depends on the composition of the Re<sub>*n*</sub>Pt<sub>*m*</sub> (*n* + *m* = 5) clusters, ranging from one polaron (Re<sub>1</sub>Pt<sub>4</sub> cluster) to three polarons (Re<sub>5</sub> cluster). The reduced Ti atoms exhibit a spin magnetic moment of 0.80–0.85 μ<sub>B</sub>, which serve as a parameter to characterize Ti<sup>3+</sup> atoms. Interestingly, the Re<sub>4</sub>Pt<sub>1</sub> cluster has one of its polarons in the subsurface, which also happens in titania with oxygen vacancies.<sup>67</sup> To conclude, supported Re<sub>*n*</sub>Pt<sub>*m*</sub> (*n* + *m* = 5) clusters hold polarons to the surface due to the electrostatic attraction, making them more available for chemical reactions than polarons formed through vacancies.<sup>68</sup>



Fig. 3b shows the projected density of states (PDOS) of  $\text{Re}_n\text{Pt}_m$  ( $n + m = 5$ ) clusters supported on  $\text{TiO}_2(110)$ , where the cluster and polaron states have been multiplied by six to ease the observation. Polaron states (3d states of  $\text{Ti}^{3+}$ ) are shown in yellow and are located about 1 eV below the conduction band of  $\text{TiO}_2(110)$ . As the number of polarons increases, the intensity of defect states is higher. The  $\text{Re}_5$  cluster produces three polarons and has a higher intensity of  $\text{Ti}^{3+}$  states. In contrast, the supported  $\text{Pt}_5$  cluster does not have states corresponding to a reduced Ti atom, which is consistent with the fact that they do not form polarons. Finally, the  $\text{Re}_4\text{Pt}_1$  cluster has two orange peaks in the gap, corresponding to the surface and subsurface polarons. Furthermore, the  $\text{Ti}^{3+}$  3d<sup>1</sup> states are coupled to lattice distortions. To analyze this structural effect without interference from other interactions, we measured lattice distortions for polarons that are not in direct interaction with the cluster. This was done to avoid any interference from the metal-substrate interaction, which also produces a distortion of the surface. We found that for supported  $\text{Re}_5$ , a polaron was identified in close proximity to the cluster, exhibiting an elongation of the Ti–O bond (0.13–0.18 Å) when the oxygens were bound to the Ti cation hosting the polaron. For other clusters, polaron formation was accompanied by a lattice distortion of approximately 0.15 Å known as a phonon cloud. An alternative explanation is that the interaction between the cluster and the surface results in the reduction of Ti atoms in the substrate (from a  $\text{Ti}^{4+}$  cation to  $\text{Ti}^{3+}$ ), which causes distortions in the lattice due to the increase in the ionic radius. In a similar vein, Lopez-Caballero *et al.* reported a distortion of this nature for small polarons induced by the  $\text{Ag}_5$  cluster supported on  $\text{TiO}_2(110)$ .<sup>42</sup> Therefore, we can conclude that in the case of Pt–Re mixed clusters, the cluster–surface interaction is responsible for the formation of small polarons.<sup>69</sup>

### 3.2 Adsorption and activation of $\text{O}_2$ by gas-phase and supported $\text{Re}_n\text{Pt}_m$ clusters

Next, we will study the molecular adsorption and dissociation of  $\text{O}_2$  on  $\text{Re}_n\text{Pt}_m$  ( $n + m = 5$ ) clusters, both free and supported on  $\text{TiO}_2(110)$ . The  $\text{O}_2$  molecule can adsorb in three different states, as molecular oxygen ( $\text{O}_2$ ), superoxo ( $\text{O}_2^-$ ), or peroxy ( $\text{O}_2^{2-}$ ). Calculations performed with our DFT model for the gas-phase  $\text{O}_2$  molecule yielded a bond distance (1.23 Å), magnetic moment ( $2.0\mu_B$ ), and stretching vibration ( $1564\text{ cm}^{-1}$ ) consistent with experiments.<sup>70</sup> These results support the methodology employed for the  $\text{O}_2$  activation in the current study. The chemical adsorption of  $\text{O}_2$  is characterized by a charge transfer from the catalyst to the oxygen molecule, forming superoxo or peroxy species. One possible way of identifying superoxo and peroxy species is to use the stretching frequency of the molecule (below about  $900\text{ cm}^{-1}$  for peroxy and about  $900\text{ cm}^{-1}$  for superoxo), although the boundary is not clear.<sup>14</sup> The assignment of a species for adsorbed  $\text{O}_2$  depends on various electronic and structural parameters. According to experimental reports,<sup>10</sup> the superoxide shows an O–O bond elongation (1.35 Å), a decrease in magnetization ( $1.0\mu_B$ ), and a shift of the stretching frequency ( $1100\text{ cm}^{-1}$ ) with respect to the neutral

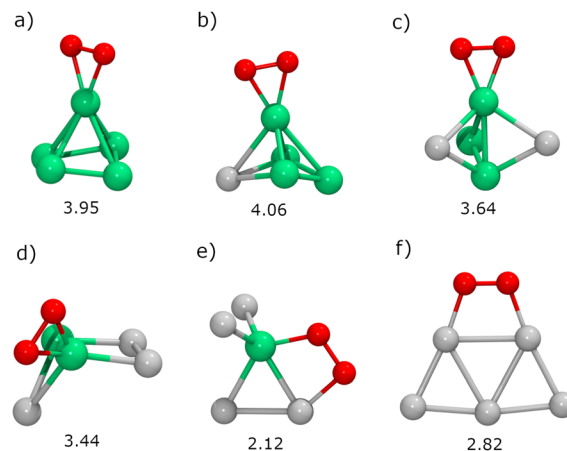


Fig. 4 The most stable structures for  $\text{O}_2$  adsorption on gas-phase  $\text{Re}_n\text{Pt}_m$  ( $n + m = 5$ ) clusters: (a)  $\text{Re}_5$ , (b)  $\text{Re}_4\text{Pt}_1$ , (c)  $\text{Re}_3\text{Pt}_2$ , (d)  $\text{Re}_2\text{Pt}_3$ , (e)  $\text{Re}_1\text{Pt}_4$ , (f)  $\text{Pt}_5$ . The adsorption energy ( $E_{\text{ads}}$ ) is displayed below each structure in eV.

molecule. Finally, peroxy is a non-magnetic species with more drastic O–O bond stretching ( $\nu = 877\text{ cm}^{-1}$ ,  $r = 1.48\text{ Å}$ ).

In gas-phase  $\text{Re}_n\text{Pt}_m$  clusters with five atoms, the adsorption energy for  $\text{O}_2$  ranges from 2.12 to 4.06 eV, indicating a strong interaction between the molecule and the  $\text{Re}_n\text{Pt}_m$  clusters (Fig. 4). In all cases, the  $\text{O}_2$  molecule has a strong preference towards binding at the Re sites. The highest adsorption energy was obtained for clusters with significant Re content, such as  $\text{Re}_5$ ,  $\text{Re}_4\text{Pt}_1$ ,  $\text{Re}_3\text{Pt}_2$ , and  $\text{Re}_2\text{Pt}_3$ , which exhibit their most stable structure in the  $\eta^2$ -Re mode. The significant adsorption energies of  $\text{O}_2$  suggest that desorption is unlikely, particularly in Re-rich clusters. On the other hand,  $\text{Re}_1\text{Pt}_4$  and  $\text{Pt}_5$  clusters prefer bridging-type adsorption ( $\mu_2$ ), with much lower  $\text{O}_2$  binding energies compared to the case of Re-rich clusters. Wang *et al.* have studied the adsorption of  $\text{O}_2$  on pure Pt clusters, with  $\text{Pt}_4$  and  $\text{Pt}_6$  clusters also showing a bridge-like adsorption mode for molecular  $\text{O}_2$ .<sup>71</sup> The  $\text{O}_2$  molecule adsorbed on  $\text{Re}_n\text{Pt}_m$  clusters has a bond length ranging from 1.40 to 1.48 Å, a stretching frequency varying from  $644$  to  $914\text{ cm}^{-1}$ , and a magnetic moment close to zero (Table 1). These values suggest that, for all the gas-phase  $\text{Re}_n\text{Pt}_m$  clusters,  $\text{O}_2$  binds as a peroxy species, indicating a strong activation of the O–O bond upon molecular adsorption.

In supported  $\text{Re}_n\text{Pt}_m$  ( $n + m = 5$ ) clusters, the adsorption energy for  $\text{O}_2$  varies from 1.37 to 3.65 eV (Fig. 5). Therefore, in all cases the clusters supported on  $\text{TiO}_2(110)$  exhibit a lower adsorption energy compared to the gas-phase clusters. Several factors contribute to this decrease in reactivity, the most important being the bonding of metal atoms to the surface oxygen atoms. This surface effect is particularly clear in the cases of  $\text{Re}_4\text{Pt}_1$  and  $\text{Re}_3\text{Pt}_2$ ; for those clusters the oxygen molecule binds at Re sites which are already forming strong O–Re bonds to the substrate, and this has a high energetic cost of approximately 1.5 eV. Another effect is the transition from 2D geometries (in the unsupported case) to 3D ones for supported clusters; in the case of the  $\text{Pt}_5$  cluster, we find a decrease of  $\text{O}_2$  binding energy of almost 1 eV. As it happened



**Table 1** The O–O bond lengths ( $r_{\text{O-O}}$ , in Å), O–O stretching frequencies ( $\nu_{\text{O-O}}$ , in  $\text{cm}^{-1}$ ), and magnetic moments ( $M_{\text{O}_2}$ , in  $\mu_{\text{B}}$ ) for  $\text{O}_2$  adsorbed on the  $\text{Re}_n\text{Pt}_m/\text{TiO}_2(110)$  systems

Sites	Parameters	$\text{Re}_5$	$\text{Re}_4\text{Pt}_1$	$\text{Re}_3\text{Pt}_2$	$\text{Re}_2\text{Pt}_3$	$\text{Re}_1\text{Pt}_4$	$\text{Pt}_5$
Gas-phase cluster	$r_{\text{O-O}}$	1.46	1.47	1.48	1.47	1.48	1.40
	$\nu_{\text{O-O}}$	914	909	898	908	644	758
	$M_{\text{O}_2}$	0.13	0.07	0.03	0.02	0.21	0.05
Supported cluster	$r_{\text{O-O}}$	1.50	1.46	1.32	1.45	1.34	1.40
	$\nu_{\text{O-O}}$	680	925	1164	938	1099	831
	$M_{\text{O}_2}$	0.00	0.09	0.01	0.00	0.77	0.22
Surface site	$r_{\text{O-O}}$	1.45	1.45	1.41	1.45	1.41	1.45
	$\nu_{\text{O-O}}$	951	962	934	957	931	960
	$M_{\text{O}_2}$	0.00	0.00	0.00	0.00	0.00	0.02
Interface site	$r_{\text{O-O}}$	—	—	1.41	1.39	1.41	1.40
	$\nu_{\text{O-O}}$	—	—	881	893	843	837
	$M_{\text{O}_2}$	—	—	0.04	0.00	0.02	0.00

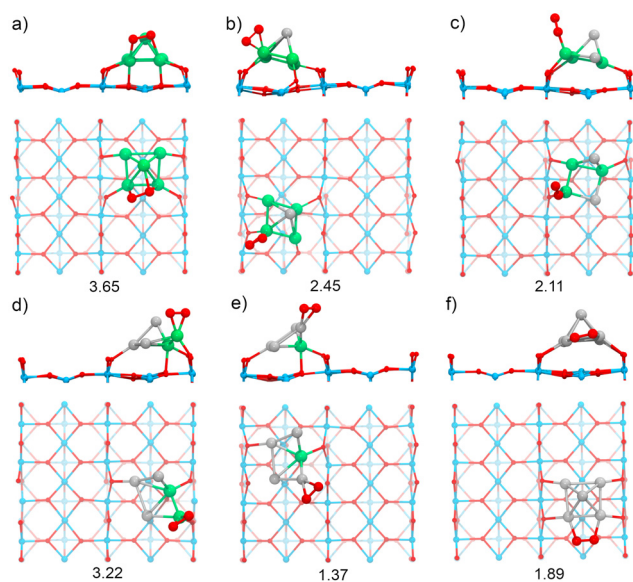


**Fig. 5** The most stable structures for  $\text{O}_2$  adsorption on  $\text{Re}_n\text{Pt}_m$  ( $n + m = 5$ ) clusters supported on  $\text{TiO}_2(110)$  (Side and top views are displayed): (a)  $\text{Re}_5$ , (b)  $\text{Re}_4\text{Pt}_1$ , (c)  $\text{Re}_3\text{Pt}_2$ , (d)  $\text{Re}_2\text{Pt}_3$ , (e)  $\text{Re}_1\text{Pt}_4$ , (f)  $\text{Pt}_5$ . The adsorption energy ( $E_{\text{ads}}$ ) is displayed below each structure in eV. For ease of analysis, only the last layer is shown in the simplified side view of the supported clusters.

for clusters in the gas phase, we find a clear trend for higher  $\text{O}_2$  adsorption energies in the case of clusters with a high concentration of Re, whereas  $\text{Pt}_5$  and  $\text{Re}_1\text{Pt}_4$  clusters have much lower adsorption energies. The most stable adsorption modes on the supported clusters are: mono ( $\eta^1\text{-Re}$ ), top ( $\eta^2\text{-Pt}$ ,  $\eta^2\text{-Re}$ ), and bridge ( $\mu_3\text{-Re}$ ,  $\mu_2\text{-Pt}$ ) types. The high fluxionality of the supported clusters results in important structural changes taking place upon adsorption of the  $\text{O}_2$  molecule. This effect is particularly strong for the  $\text{Re}_3\text{Pt}_2$  and  $\text{Re}_2\text{Pt}_3$  clusters, where the Re atom that interacts with  $\text{O}_2$  experiences a significant displacement, and the square pyramid distorts into a more open conformation. The  $\text{O}_2$  on supported  $\text{Re}_n\text{Pt}_m$  clusters has a bond length from 1.32 to 1.50 Å, a stretching frequency between

680 and 1164  $\text{cm}^{-1}$ , and a magnetic moment from 0.00 to 0.77  $\mu_{\text{B}}$  (see Table 1, which reports all the parameters for the adsorbing  $\text{O}_2$  molecule in gas-phase and  $\text{TiO}_2$ -supported clusters). These parameters can be related to superoxo (for  $\text{Re}_3\text{Pt}_2$  and  $\text{Re}_1\text{Pt}_4$ ) and peroxy species (for the rest of clusters), with the highest O–O bond activation taking place on  $\text{Re}_5$ ,  $\text{Re}_4\text{Pt}_1$ , and  $\text{Re}_2\text{Pt}_3$  clusters, consistent with the highest adsorption energies.

The Bader charge analysis was performed on the most stable structures to understand the activation of  $\text{O}_2$  on gas-phase and supported  $\text{Re}_n\text{Pt}_m$  clusters. Previous theoretical studies have shown that the charge transfer from the cluster to  $\text{O}_2$  depends on the adsorption mode.<sup>55,72</sup> Fig. 6 shows the relationship between the charge received by  $\text{O}_2$  and the O–O bond length, with the data labeled according to the adsorption mode. There is a linear relationship between the charge and bond length of  $\text{O}_2$ , with only the  $\eta^1\text{-Re}$  and  $\mu_2\text{-RePt}$  modes showing some sizable discrepancies from the linear dependency. The  $\text{O}_2$  molecule receives a charge ranging from 0.44 to 0.99 e, with the sites which transfer the largest amount of charge being Re atoms (cyan, green), results which are consistent with the larger intrinsic reactivity of these sites. The  $\mu_3\text{-Re}$  and  $\eta^2\text{-Re}$  adsorption modes exhibited a magnetic moment of  $\text{O}_2$  close to zero, suggesting a full occupation of the  $\pi^*$  antibonding orbitals of the molecule. In contrast, when  $\text{O}_2$  adsorbs on Pt atoms charge transfer decreases and the magnetic moment increases, a fact which correlates with the lower adsorption energies at those sites. Therefore, charge transfer on  $\text{O}_2$  gives a good measure of the activation of the O–O bond.

An analysis was conducted on the charge of the supported clusters both before and after  $\text{O}_2$  adsorption, as well as the charge of each atom within the cluster (ESI,† Table S1). After adsorption of  $\text{O}_2$ , the total positive charge on the Re–Pt clusters increases as a result of the charge transfer to the oxygen molecule. Also, we find that the metal atoms directly bonded to  $\text{O}_2$  are the ones who transfer the majority of the electronic charge to the oxygen molecule. The larger intrinsic reactivity of the Re atoms results in larger charge transfers, compared to Pt.

In Fig. 6b, we have also analyzed the PDOS for  $\text{O}_2$  adsorption on supported  $\text{Re}_5$  and  $\text{Re}_1\text{Pt}_4$ , which are the two clusters with the highest and lowest  $\text{O}_2$  binding energy, respectively. The first panel shows the PDOS of gas-phase  $\text{O}_2$ , and the two panels below show the PDOS for these two supported clusters. For gas-phase  $\text{O}_2$ , the  $\pi^*$  antibonding orbitals split into occupied spin-up and unoccupied spin-down states, resulting in a triplet spin state and a magnetic moment of  $2\mu_{\text{B}}$ . Once the half-occupied  $\pi^*$  orbitals are filled, the spin splitting and the magnetic moment disappear.<sup>73</sup> When  $\text{O}_2$  adsorbs at the supported clusters, there are significant differences between the Re-rich and Pt-rich cases. During the adsorption process the 2p-states of the molecule overlap with the 5d-states of the metal atoms, leading to chemisorption of  $\text{O}_2$ . In the case of  $\text{Re}_1\text{Pt}_4$ , the  $\text{O}_2$  states of retain spin splitting and have a DOS similar to the superoxo species,<sup>74</sup> with antibonding  $\pi^*$  orbitals being unoccupied just above the Fermi level. For the  $\text{Re}_5$  cluster the  $\pi^*$  antibonding orbitals are fully occupied, and become symmetric for spin up



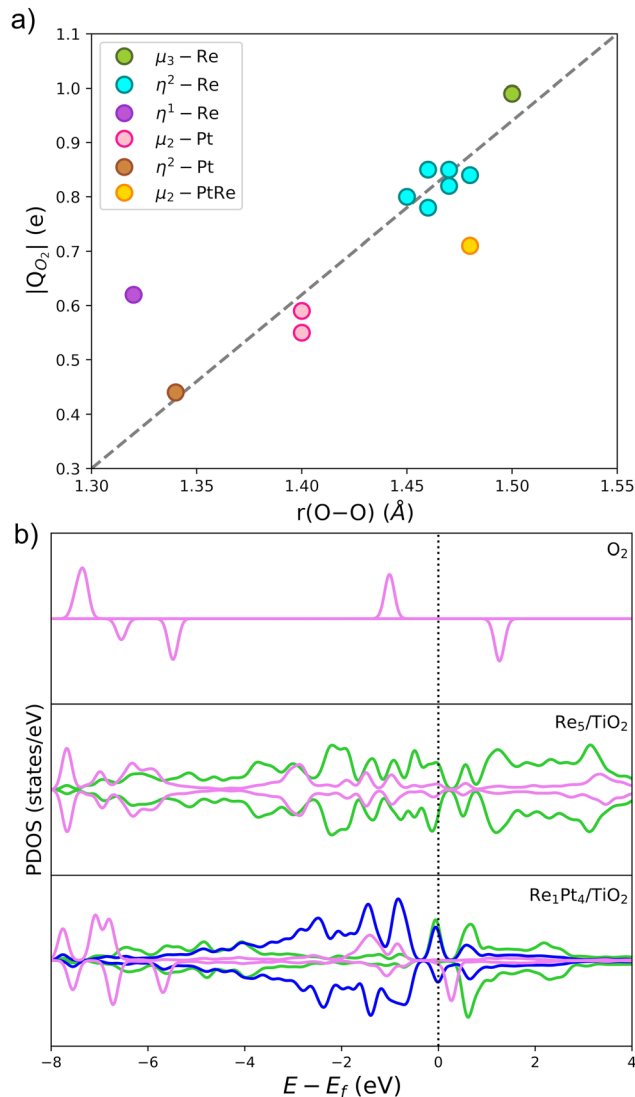


Fig. 6 Electronic properties for  $O_2$  activation on metal cluster sites. (a) Relationship between  $O_2$  charge and O–O length for  $O_2$  adsorption on  $Re_nPt_m$  systems. These data correspond to the most stable sites on the gas-phase and supported clusters. (b) The projected density of states (PDOS) of the  $O_2$  adsorption on  $Re_5$  and  $Re_1Pt_4$  supported clusters. The first panel shows the PDOS of gas-phase  $O_2$ , and the two panels below are the PDOS for the systems with higher and lower adsorption energy. The 5d states of Re, 5d states of Pt, and 2p states of  $O_2$  are represented by green, blue, and pink, respectively.

and spin down, consistent with a peroxo state with the magnetic moment equal to zero. This comparison of the electronic structure for both compositions correlates with the larger cluster- $O_2$  charge transfer and much higher adsorption energy in the case of the Re-rich stoichiometry.

Next, we studied the dissociation of  $O_2$  over the metal clusters, comparing the results for both gas-phase clusters, and clusters supported on  $TiO_2(110)$ . In each case, the starting point for the dissociation was taken from the most stable site of molecular  $O_2$  adsorption. Table 2 summarizes all the results, showing the values of the activation energies  $E_{act}$ , the reaction energies  $\Delta E$  and the imaginary frequencies of the transition

Table 2 The activation barriers ( $E_{act}$ , eV), the reaction energies ( $\Delta E$ , eV), and imaginary frequencies of the transition states ( $\nu_i$ ,  $cm^{-1}$ ) for the dissociation of  $O_2$  on the metal cluster site of gas- and supported-phases. In the gas-phase  $Re_5$  cluster, the reaction path exhibits a continuously decreasing energy, resulting in the absence of a transition state (TS)

	Gas-phase clusters			Supported clusters		
	$E_{act}$	$\Delta E$	$\nu_i$	$E_{act}$	$\Delta E$	$\nu_i$
$Re_5$	—	−3.52	—	0.02	−2.92	415
$Re_4Pt_1$	0.41	−3.23	561	0.98	−3.25	224
$Re_3Pt_2$	0.18	−2.87	598	0.37	−3.43	216
$Re_2Pt_3$	0.53	−2.87	789	0.60	−3.10	579
$Re_1Pt_4$	0.05	−2.83	347	0.47	−1.41	136
$Pt_5$	0.24	−0.44	254	0.61	−0.18	174

states, for both gas-phase and supported clusters. The reaction energies  $\Delta E$  are defined as the energy difference between the initial state (with molecular  $O_2$  bonded to the cluster) and the final state (with two separated O adatoms). For unsupported clusters, reaction energies are always large, of the order of 3 eV, with the sole exception of the pure  $Pt_5$  cluster. This means that oxygen dissociation is highly exothermic, and dissociative adsorption is strongly favoured whenever there is at least one reactive Re atom in the cluster. In the absence of reactive Re atoms, the reaction energy for  $Pt_5$  decreases to only −0.44 eV. Additionally, we calculated the free energy for the dissociation reaction at 300 K and 1 atm on  $Re_nPt_m$  ( $n + m = 5$ ) gas-phase clusters (see data in Table S4 of the ESI†). In most cases, the thermal correction contributes less than 0.1 eV to the reaction energy. Thus, we observed that the trends remain consistent when considering the free energy at 300 K. Thus, this correction has no impact on our analysis.

For gas-phase clusters, the reaction path for  $O_2$  dissociation is shown in Fig. 7. In all cases, activation barriers are low, in the range of 0.0–0.5 eV. The low value of the barrier and the large energy gain for dissociation of  $O_2$  causes that, in general, the transition state was found for very small expansions of the O–O bond. In the case of pure  $Re_5$ , the barrier is extremely small, virtually non-existent, and we were not able to properly identify a transition state. The corresponding results for clusters supported on the  $TiO_2(110)$  surface are shown in Fig. 8. Activation barriers are slightly larger, although they never exceed 1 eV. Again, dissociation of  $O_2$  on pure  $Re_5$  takes place almost spontaneously, with only a residual barrier of 0.02 eV. The interaction of the surface with the cluster causes some important changes in the mechanisms for  $O_2$  dissociation for some compositions; for pure  $Pt_5$ , the supported cluster undergoes a drastic configuration change after oxygen dissociation and loses bonds at the metal-substrate interface. Reaction energies for supported clusters are, in general, similar to the ones found for gas-phase cluster, with one very important exception, the  $Re_1Pt_4$  cluster. When this cluster is supported, the reaction energy drops from 2.8 to 1.4 eV. This effect is caused by the binding of the Re atom to the substrate, which serves as an anchoring point. Since this atom is inaccessible to the adsorbed  $O_2$  molecule (as there are several Pt atoms on top of it), dissociation must take place at less reactive Pt sites, with an



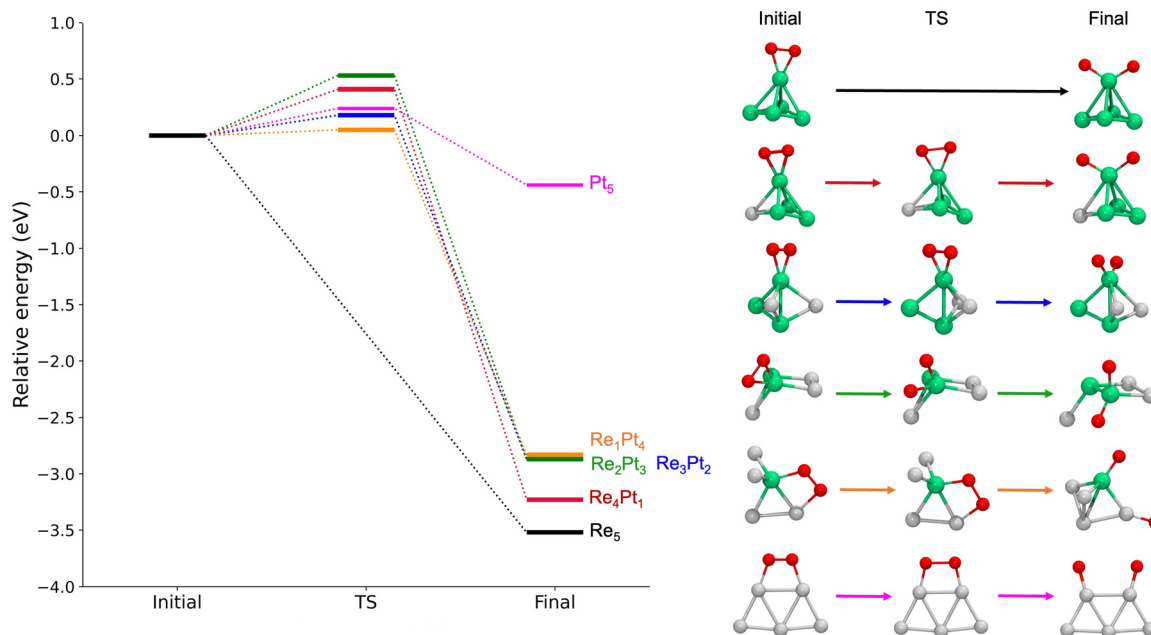


Fig. 7 Left panel: Reaction energetics for the dissociation of  $\text{O}_2$  on gas-phase  $\text{Re}_7\text{Pt}_m$  clusters. All the energies are shown relative to the one of the initial state, on each case. Right panel: Structures for initial, transition and final states for each cluster. The colors of the atoms are consistent with those in previous figures.

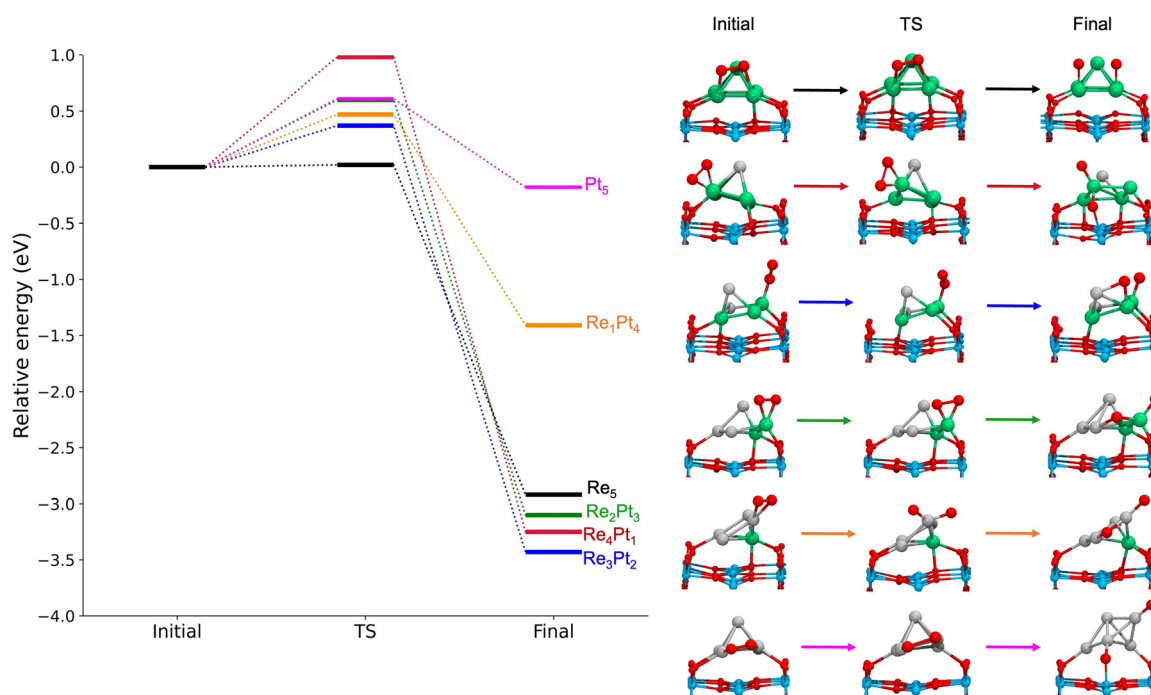


Fig. 8 Left panel: Reaction energetics for the dissociation of  $\text{O}_2$  on supported  $\text{Re}_7\text{Pt}_m$  clusters. All the energies are shown relative to the one of the initial state, on each case. Right panel: Structures for initial, transition and final states for each cluster. The colors of the atoms are consistent with those in previous figures.

important energetic cost. Overall, the results show that for all compositions dissociation of  $\text{O}_2$  is an exothermic process with low activation barriers. Nevertheless, there are important quantitative differences between Re-rich clusters, much more

reactive, and Pt-rich ones; whenever the reactive Re sites are not available, sizable changes in reactivity will occur.

We have analyzed the charge transfer to  $\text{O}_2$  when it adsorbs on  $\text{TiO}_2$ -supported clusters (see data in Table S3 of the ESI<sup>†</sup>). In





all the cases, almost all the charge is donated from the 5d-states of the metal clusters, with the charge donated from the  $\text{TiO}_2$  substrate being very small. Finally, we also studied the most stable conformations for the two dissociated oxygen adatoms on both gas-phase and supported clusters. The results are shown in Fig. S4 of the ESI.† In many cases, diffusion of oxygen atoms towards more stable locations is linked to strong conformational changes in the cluster. This happens both for unsupported and for supported clusters. Also, it must be noted that, with respect to the final states reported on Fig. 8, there is a consistent tendency towards separation of the oxygen adatoms; initially, these are bonded to the same atom, but a large energy gain takes place when each one binds at a separate metal site.

### 3.3 Adsorption of $\text{O}_2$ to surface sites of $\text{TiO}_2$ substrate

We will now study the adsorption of  $\text{O}_2$  to surface sites of the  $\text{TiO}_2$  substrate, separated some distance from  $\text{Re}_n\text{Pt}_m$  clusters previously deposited on the surface. First, we have checked that on the pristine  $\text{TiO}_2$  surface (that is, without metal clusters supported on it)  $\text{O}_2$  adsorption is very weak ( $E_{\text{ads}} = 0.11$  eV), which is in agreement with other theoretical studies.<sup>37,75</sup> On the contrary, Sokolovic *et al.* reported that the reduced  $\text{TiO}_2(110)$  surface can adsorb the oxygen molecule.<sup>76</sup> The presence of oxygen vacancies leads to the formation of small polarons located on the next-nearest subsurface  $\text{Ti}_{6c}$  atoms. These polarons transfer charge to the adsorbed  $\text{O}_2$  molecule, resulting in the formation of the peroxo species and atomic oxygen.<sup>76</sup>

Similar to the case of reduced  $\text{TiO}_2(110)$  surface with oxygen vacancies, the pristine  $\text{TiO}_2$  surface with  $\text{Re}_n\text{Pt}_m$  clusters supported on it also contains small surface polarons. Previously, our analysis of the electronic structure of the  $\text{Re}_n\text{Pt}_m/\text{TiO}_2(110)$  system has shown that the metal clusters transfer electrons to the surface, leading effectively to the reduction of  $\text{Ti}_{5c}$  atoms. Consequently, we find that in the presence of supported metal clusters the  $\text{O}_2$  can adsorb on surface  $\text{Ti}_{5c}$  with moderately strong adsorption energies, ranging from 0.93 to 1.55 eV (ESI,† Table S2). In general, adsorption of  $\text{O}_2$  is slightly stronger in the case of Re-rich clusters; the stronger cluster–surface interaction and larger charge transfer also results in stronger  $\text{O}_2$ – $\text{TiO}_2$  interactions. In the case of supported  $\text{Pt}_5$  and  $\text{Re}_1\text{Pt}_4$ , the adsorption energies of  $\text{O}_2$  on the surface  $\text{Ti}_{5c}$  sites are comparable to the ones obtained when  $\text{O}_2$  adsorbs at these clusters. This means that  $\text{O}_2$  adsorption on the surface may be significant for these compositions. Also, the process of  $\text{O}_2$  spillover from the supported cluster to the substrate is feasible, given the similar stability of molecular  $\text{O}_2$  at both sites. In contrast, for Re-rich compositions, the adsorption energy of  $\text{O}_2$  is much higher at the metal sites. This fact, together with the very high reaction energy for  $\text{O}_2$  dissociation at the Re-rich clusters, implies that any  $\text{O}_2$  molecule that could diffuse from surface sites to the cluster will remain there, being dissociated afterwards.

Depending on the cluster composition, we found two competing adsorption modes: a  $\eta^2$ -Ti mode which displaces vertically the  $\text{Ti}_{5c}$  atom from the surface by about 1 Å, and a  $\mu_2$ -Ti

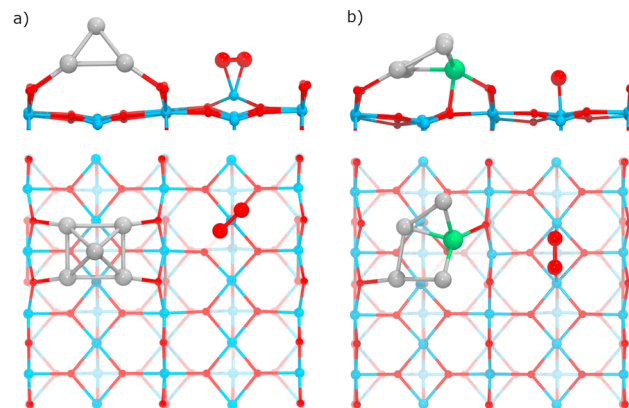


Fig. 9 Relaxed structures for  $\text{O}_2$  adsorption on the  $\text{TiO}_2(110)$  surface in the presence of supported  $\text{Re}_n\text{Pt}_m$  clusters. (a) The  $\eta^2$ -Ti mode on the surface site ( $\text{Pt}_5$  supported system). (b) The  $\mu_2$ -Ti mode on the surface site ( $\text{Re}_1\text{Pt}_4$  supported system).

mode where  $\text{O}_2$  bridges two surface  $\text{Ti}_{5c}$  sites, with very small vertical displacements for both  $\text{Ti}_{5c}$  sites. Fig. 9 shows the relaxed structures for these adsorption modes, for the supported  $\text{Re}_1\text{Pt}_4$  and  $\text{Pt}_5$  clusters. The O–O bond lengths for each of these two modes are 1.45 and 1.41 Å, respectively (see Table 1). The stretching frequency for the adsorbed  $\text{O}_2$  molecule ranges from 931 to 962  $\text{cm}^{-1}$ , and its magnetic moment is always equal to zero. These facts indicate that the  $\text{O}_2$  molecule adsorbs to  $\text{Ti}_{5c}$  surface sites as a peroxo species.

We have also analyzed the electronic structure of molecular  $\text{O}_2$  adsorbed at  $\text{Ti}_{5c}$  surface sites. Table S3 in the ESI† shows the charge transfer to the  $\text{O}_2$  molecule, for each of the co-adsorbed  $\text{Re}_n\text{Pt}_m$  clusters. The values are fairly uniform, ranging from 0.88 to 0.94 electrons. It is interesting to compare the results for  $\text{O}_2$  adsorption to the metal atoms of the cluster with adsorption of  $\text{O}_2$  at surface  $\text{Ti}_{5c}$  sites. When  $\text{O}_2$  adsorbs at the  $\text{TiO}_2$  substrate, some part of the charge donated to oxygen is transferred from the substrate, and other part from the cluster. Interestingly, the amount of charge transferred from the surface decreases as the amount of Pt in the cluster increases. We also calculated the PDOS of bimetallic Re–Pt clusters after the  $\text{O}_2$  adsorption on the surface and analyzed the electronic states of the reduced Ti atoms in the substrate. To enhance the clarity of the plots, we multiplied the  $\text{Ti}^{3+}$ , the  $\text{O}_2$  molecule and metal clusters states by ten in the PDOS (Fig. 10). The 5d-states of Pt and Re exhibit minor changes because they do not participate directly on the  $\text{O}_2$  bonding. The displayed states only show spin up as there is no spin splitting. The 3d states of  $\text{Ti}^{3+}$  for  $\text{Re}_3\text{Pt}_2$  and  $\text{Re}_1\text{Pt}_4$  systems disappear, indicating a charge transfer from  $\text{Ti}^{3+}$  atoms to the  $\text{O}_2$  molecule. Although the other systems retain some polaronic states, there is a significant reduction. This was verified by analyzing the magnetic moment of the Ti atoms, where only one or no polaron remains after adsorption. Thus,  $\text{Ti}^{3+}$  atoms facilitate the adsorption of  $\text{O}_2$  on the surface by transferring electrons to the molecule.

Finally, we have considered the possibility of dissociation of the  $\text{O}_2$  molecule adsorbed at  $\text{Ti}_{5c}$  surface sites. The results in Fig. 10b show that this is a very endothermic process. Barriers



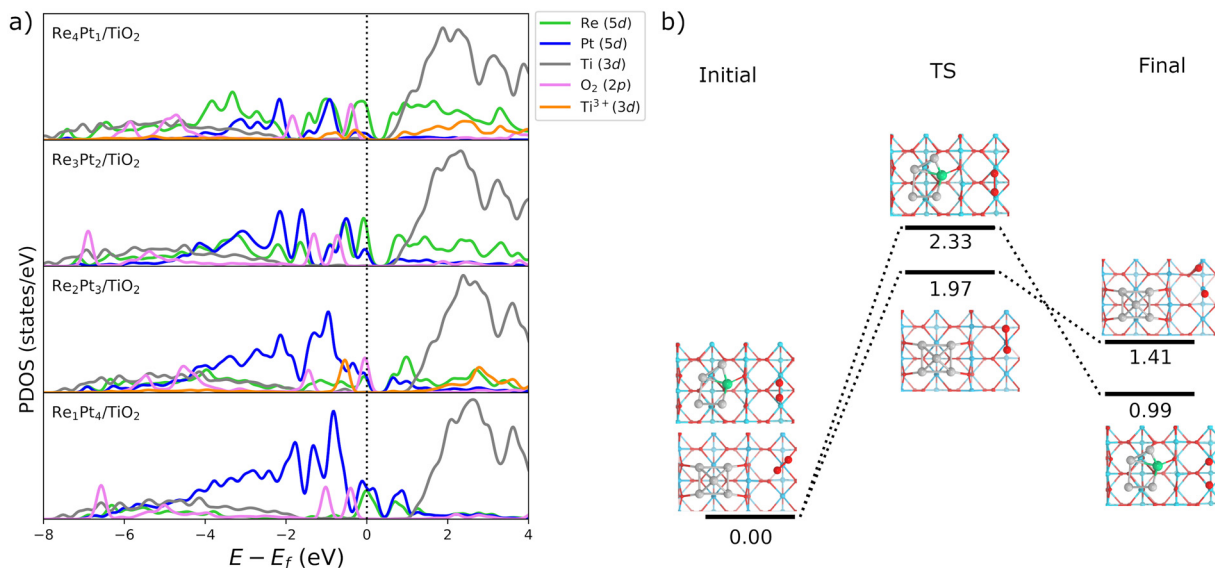


**Fig. 10** (a) Projected density of states (PDOS) for  $\text{O}_2$  adsorbed on the  $\text{TiO}_2(110)$  surface in the presence of supported  $\text{Re}_n\text{Pt}_m$  clusters. The 5d states of Re, 5d states of Pt, 3d states of  $\text{Ti}^{4+}$ , 3d states of  $\text{Ti}^{3+}$ , and 2p states of  $\text{O}_2$  are represented by green, blue, gray, orange, and pink, respectively. The  $\text{Ti}^{3+}$ , the  $\text{O}_2$  molecule, and metal clusters states are multiplied by ten in the PDOS. (b) Energetic barriers for the dissociation of  $\text{O}_2$  on  $\text{TiO}_2(110)$  surface in the presence of supported  $\text{Pt}_5$  and  $\text{Re}_1\text{Pt}_4$  clusters.

for  $\text{O}_2$  dissociation on the surface were calculated in the case of coadsorbed  $\text{Pt}_5$  and  $\text{Re}_1\text{Pt}_4$  systems. In both cases, energy barriers are very high (1.97 and 2.33 eV), leading to final states at least 1 eV higher in energy than the initial state with the  $\text{O}_2$  molecule intact. This contrasts with the experimental observation of atomic oxygen on the surface with oxygen vacancies.<sup>76</sup> Therefore, on surface sites around the Re–Pt supported clusters  $\text{O}_2$  only experiments a mild activation to a peroxo state, with complete dissociation being unfeasible due to the large barriers involved.

### 3.4 Adsorption and activation of $\text{O}_2$ by the metal-support interface

Finally, we have investigated the adsorption and dissociation of  $\text{O}_2$  at interfacial cluster- $\text{TiO}_2$  sites, with the  $\text{O}_2$  molecule forming bonds with both  $\text{Ti}_{5c}$  surface atoms and Pt or Re atoms in the supported cluster. These types of catalytic sites are extremely important for a variety of systems and reactions. On one hand, stability of adsorbates at these locations determines if processes of spillover from the cluster to the substrate are feasible (or conversely, reverse spillover from the substrate to the cluster). On the other hand, these sites are the natural meeting place for different reactants which prefer to bind either at the supported cluster, or at the substrate. As a consequence, for many oxidation reactions these sites are believed to be the active sites where the reaction takes place.<sup>77,78</sup> Fig. 11a shows the most stable conformations found for molecular  $\text{O}_2$  adsorbed at the cluster-support interface for  $\text{Re}_3\text{Pt}_2$ ,  $\text{Re}_2\text{Pt}_3$ ,  $\text{Re}_1\text{Pt}_4$ , and  $\text{Pt}_5$  clusters. For all these compositions, the molecule adsorbs bridging a  $\text{Ti}_{5c}$  atom in the surface and a Pt atom within the cluster. For  $\text{Re}_5$  and  $\text{Re}_4\text{Pt}_1$ , the cluster-support interface is composed exclusively by Re atoms. In these cases, when we relaxed initial starting geometries with  $\text{O}_2$  bridging Ti

and Re sites, we found that the  $\text{O}_2$  molecule spontaneously dissociates into an oxygen atom bonded to the Re sites in the cluster and another oxygen atom which remains bonded to the  $\text{Ti}_{5c}$  surface site (see Fig. S5 in the ESI†). It is interesting to compare the binding energies of the final states with one O atom adsorbed at the substrate (4.43 and 5.12 eV for  $\text{Re}_5$  and  $\text{Re}_4\text{Pt}_1$ , respectively) with the corresponding values where the two oxygen adatoms remain bonded to the Re-rich clusters (7.74 and 6.65 eV for the most stable conformations on each case). Clearly, there is a high energetic cost against spillover of dissociated oxygen atoms to the substrate, in the case of Re-rich clusters.

The adsorption energies at Pt sites vary in a range between 1.41 to 2.05 eV. Such binding strength is similar to the values found for  $\text{O}_2$  bound at the supported Pt-rich clusters, and it is only slightly larger than the values found at the  $\text{Ti}_{5c}$  surface sites away from the cluster. The most stable adsorption modes are  $\mu_2$ -TiPt and  $\mu_3$ -TiPt with O–O length ranging from 1.39 to 1.41 Å. At the interface,  $\text{O}_2$  has a stretching frequency varying between 837 and 893  $\text{cm}^{-1}$ , and a magnetic moment equal to zero (see Table 1). Therefore, adsorption of  $\text{O}_2$  at these sites takes place as a peroxo species. The charge transfer to the  $\text{O}_2$  molecule is fairly constant, between  $-0.83$  and  $-0.88$  electrons. Part of this extra charge is transferred from the substrate, but the majority is donated by the supported cluster (see Table S3 in the ESI†).

Finally, we have calculated the energy barriers for  $\text{O}_2$  dissociation at the interface of supported Pt-rich clusters ( $\text{Pt}_5$  and  $\text{Re}_1\text{Pt}_4$ , see Fig. 11b). We find that oxygen atom dissociates on the surface and the other on the Pt atoms of the cluster. The process is exothermic, and the energy barriers are similar to those found at the metal cluster site (less than 0.70 eV). Although Re does not directly participate in the dissociation



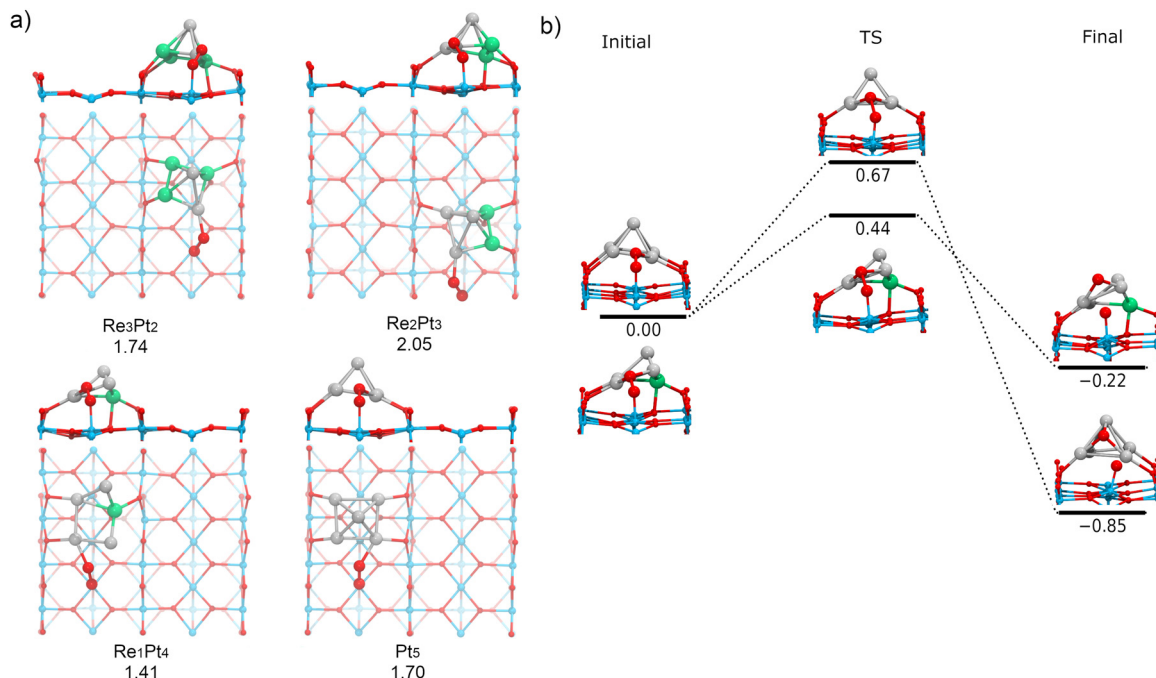


Fig. 11 O<sub>2</sub> adsorption on the Ti-Pt interface. (a) The most stable structures for O<sub>2</sub> adsorption on the interface of Re<sub>3</sub>Pt<sub>2</sub>, Re<sub>2</sub>Pt<sub>3</sub>, Re<sub>1</sub>Pt<sub>4</sub>, and Pt<sub>5</sub> supported clusters. The adsorption energy ( $E_{\text{ads}}$ ) is displayed below each structure in eV. The structure of the supported clusters is simplified by showing only the surface trilayer for ease of analysis. (b) Energetic barriers to dissociation of O<sub>2</sub> on the Ti-Pt interface of Pt<sub>5</sub> and Re<sub>1</sub>Pt<sub>4</sub> supported clusters.

of O<sub>2</sub> in this case, it can be observed that the dissociation barrier is lower for the cluster containing a Re impurity. Contrary to the case of Re-rich clusters, the energetic cost for transferring oxygen adatoms from the cluster to the TiO<sub>2</sub> substrate is not very high, which means that spillover of dissociated oxygen to the surface can take place for Pt-rich clusters. Overall, our results show that dissociation of O<sub>2</sub> at the Pt-Ti interface requires little energy, whereas the Re-Ti interface causes a dissociative adsorption of O<sub>2</sub>, leading to spontaneous production of atomic oxygen.

## 4 Conclusions

In this study, the adsorption and activation of O<sub>2</sub> on Re<sub>*n*</sub>Pt<sub>*m*</sub> ( $n + m = 5$ ) clusters, both free and supported on TiO<sub>2</sub>(110), were investigated at the metal cluster, surface, and interfacial sites. The most stable structures for the supported clusters, at various compositions, are characterized by a strong tendency for the Re atoms in the cluster to occupy positions directly in contact with the oxygen surface sites; therefore, in mixed Pt-Re clusters it is expected that Pt atoms will preferentially be displaced towards the top part of the supported cluster, while Re accumulates at the interfacial area, increasing the adhesion of the cluster to the substrate. The composition of Re<sub>*n*</sub>Pt<sub>*m*</sub> clusters can tune the formation of surface polarons, increasing the reactivity of the surface towards reactions involving charge transfer. Thus, changes in reactivity may occur due to alterations in the cluster and surface, resulting in the emergence of new active sites, including those found at the interface and on the

reduced surface. At the metal cluster sites, the Re<sub>*n*</sub>Pt<sub>*m*</sub> clusters have a strong interaction with the O<sub>2</sub> molecule, especially on the Re atoms, which are much more reactive than the Pt atoms. The O<sub>2</sub> molecule adsorbed on Re-Pt clusters exhibits parameters typical of the peroxy species. This activation of the O-O bond is caused by charge transfer from the cluster atoms to the molecule. Dissociative adsorption can occur on Re atoms due to their significant charge donation to O<sub>2</sub>. In general, oxidation is expected in Re<sub>*n*</sub>Pt<sub>*m*</sub> ( $n + m = 5$ ) clusters because the energy barriers for dissociation are low (less than 0.7 eV). Finally, the bimetallic Re<sub>1</sub>Pt<sub>4</sub> cluster exhibits a synergistic effect of the metal atoms on its stability and reactivity. The cluster is anchored on the surface by the Re atom, while the Pt atoms activate the O<sub>2</sub> molecule.

At the surface sites, the composition of Re<sub>*n*</sub>Pt<sub>*m*</sub> clusters can tune the formation of surface polarons. Re-rich clusters transfer more electrons to the TiO<sub>2</sub>(110) surface than Pt-rich clusters, resulting in increased surface reactivity. The oxygen molecule adsorbs onto Ti atoms with moderate adsorption energies (0.93–1.55 eV). The electronic and structural parameters displayed by the O<sub>2</sub> on the surface site are analogous to those of peroxy species. Due to the adsorption of oxygen, certain polarons disappear, indicating their involvement in the activation process. However, the activation of O<sub>2</sub> can be considered mild on the surface site of Re-Pt supported clusters due to the high energy requirement to break the O-O bond. This finding contrasts with experimental reports for the TiO<sub>2</sub>(110) surface with oxygen vacancies, where atomic oxygen has been observed.

At the interfacial cluster-support sites, the Re-Ti interface causes the dissociative adsorption of O<sub>2</sub>, while the Pt-Ti



interface activates the O<sub>2</sub> molecule with typical structural parameters of a peroxo species. At the Pt–Ti interface, the adsorption energies show a slight increase with respect to the surface sites. Other clusters also exhibit O<sub>2</sub> adsorption at the interface, such as Au clusters on the MgO(100)<sup>79</sup> and TiO<sub>2</sub>(101)<sup>80</sup> surfaces. Both the metal cluster and Ti surface atoms transfer charge to the O<sub>2</sub> molecule. The energy barriers for the dissociation of O<sub>2</sub> at the Pt–Ti interface are low, similar to what was found for the cluster sites. Thus, in an oxidizing atmosphere, the interfaces of Pt/TiO<sub>2</sub> and Re/TiO<sub>2</sub> may become enriched with atomic oxygen. The interface can be an active site for chemical reactions, especially for oxidation reactions that require O<sub>2</sub> activation.<sup>77</sup>

In summary, the Re<sub>n</sub>Pt<sub>m</sub> ( $n + m = 5$ ) clusters supported on TiO<sub>2</sub>(110) display three possible sites for O<sub>2</sub> adsorption: the metal cluster, the surface, and the interface. All sites transfer charge to the O<sub>2</sub> molecule and elongate the O–O bond. In these supported clusters, the metal cluster and interface sites can dissociate the O<sub>2</sub> molecule with low energy requirements, while the surface sites requires much more energy. Thus, the sites containing Re and Pt atoms, as well as the Re–Ti and Pt–Ti interfaces, are expected to be oxidized. In Re<sub>1</sub>Pt<sub>4</sub> and Pt<sub>5</sub> supported systems, the three active sites compete with each other due to their similar adsorption energies. In terms of the role of metal atoms, Re serves to anchor the cluster to the surface, while Pt is more available to interact with O<sub>2</sub>. These findings provide new insight into the activation of O<sub>2</sub> on Re–Pt clusters supported on TiO<sub>2</sub>(110) as single-cluster catalysts.

## Author contributions

Conceptualisation: AAG, ILG, LMM; formal analysis: AAG, ILG, LMM; funding acquisition: ILG, LMM; supervision: ILG, LMM; visualisation: AAG; writing – original draft: AAG; writing – review & editing: ILG, LMM.

## Conflicts of interest

There are no conflicts to declare.

## Acknowledgements

Andrés Álvarez-García gratefully thanks CONACyT-Mexico for the PhD scholarship No. 957475. Calculations were performed at the DGTIC-UNAM Supercomputing Center under Project LANCAD-UNAM-DGTIC-049. This work was supported by DGAPA-UNAM PAPIIT under Project IN106021 and CONACyT-Mexico under Project 285821. Luis M. Molina acknowledges the support from Ministerio de Ciencia e Innovación of Spain (Grant PID2022-138340OB-I00 funded by MCIN/AEI/10.13039/501100011033 and FSE+) and from the University of Valladolid (GIR Nanostructure Physics).

## Notes and references

- C. Dong, Y. Li, D. Cheng, M. Zhang, J. Liu, Y.-G. Wang, D. Xiao and D. Ma, *ACS Catal.*, 2020, **10**, 11011–11045.
- A. J. Brandt, T. D. Maddumapatabandi, D. M. Shakya, K. Xie, G. S. Seuser, S. Farzandh and D. A. Chen, *J. Chem. Phys.*, 2019, **151**, 234714.
- R. P. Galhenage, K. Xie, H. Yan, G. S. Seuser and D. A. Chen, *J. Phys. Chem. C*, 2016, **120**, 10866–10878.
- A. S. Duke, R. P. Galhenage, S. A. Tenney, P. Sutter and D. A. Chen, *J. Phys. Chem. C*, 2015, **119**, 381–391.
- K. Tomishige, Y. Nakagawa and M. Tamura, *Chin. Chem. Lett.*, 2020, **31**, 1071–1077.
- J. Xiao and R. J. Puddephatt, *Coord. Chem. Rev.*, 1995, **143**, 457–500.
- A. S. Duke, K. Xie, A. J. Brandt, T. D. Maddumapatabandi, S. C. Ammal, A. Heyden, J. R. Monnier and D. A. Chen, *ACS Catal.*, 2017, **7**, 2597–2606.
- A. S. Duke, K. Xie, A. J. Brandt, T. D. Maddumapatabandi, S. C. Ammal, A. Heyden, J. R. Monnier and D. A. Chen, *ACS Catal.*, 2017, **7**, 2597–2606.
- L. Kang, B. Wang, Q. Bing, M. Zalibera, R. Büchel, R. Xu, Q. Wang, Y. Liu, D. Gianolio, C. C. Tang, E. K. Gibson, M. Danaie, C. Allen, K. Wu, S. Marlow, L. D. Sun, Q. He, S. Guan, A. Savitsky, J. J. Velasco-Vélez, J. Callison, C. W. Kay, S. E. Pratsinis, W. Lubitz, J. Y. Liu and F. R. Wang, *Nat. Commun.*, 2020, **11**, 17–19.
- L. X. Chen, Z. Wen, Z. W. Chen, C. V. Singh and Q. Jiang, *J. Mater. Chem. A*, 2021, **9**, 11726–11733.
- C. Vogt and B. M. Weckhuysen, *Nat. Rev. Chem.*, 2022, **6**, 89–111.
- S. Dai, J. P. Chou, K. W. Wang, Y. Y. Hsu, A. Hu, X. Pan and T. Y. Chen, *Nat. Commun.*, 2019, **10**, 1–10.
- A. Trincherro, S. Klacar, L. O. Paz-Borbón, A. Hellman and H. Grönbeck, *J. Phys. Chem. C*, 2015, **119**, 10797–10803.
- M. M. Montemore, M. A. Van Spronsen, R. J. Madix and C. M. Friend, *Chem. Rev.*, 2018, **118**, 2816–2862.
- X. Li, S. Mitchell, Y. Fang, J. Li, J. Perez-Ramirez and J. Lu, *Nat. Rev. Chem.*, 2023, 754–767.
- S. Vajda, M. J. Pellin, J. P. Greeley, C. L. Marshall, L. A. Curtiss, G. A. Ballentine, J. W. Elam, S. Catillonmucherie, P. C. Redfern, F. Mehmood and P. Zapol, *Nat. Mater.*, 2009, **8**, 213–216.
- L. Liu and A. Corma, *Chem. Rev.*, 2018, **118**, 4981–5079.
- S. Baskaran, C. Q. Xu, Y. G. Wang, I. L. Garzón and J. Li, *Sci. China Mater.*, 2020, **63**, 993–1002.
- Y. Watanabe, *Sci. Technol. Adv. Mater.*, 2014, **15**, 1–12.
- B. Ni and X. Wang, *Chem. Sci.*, 2016, **7**, 3978–3991.
- C. Yao, N. Guo, S. Xi, C. Q. Xu, W. Liu, X. Zhao, J. Li, H. Fang, J. Su, Z. Chen, H. Yan, Z. Qiu, P. Lyu, C. Chen, H. Xu, X. Peng, X. Li, B. Liu, C. Su, S. J. Pennycook, C. J. Sun, J. Li, C. Zhang, Y. Du and J. Lu, *Nat. Commun.*, 2020, **11**, 4389.
- X. L. Ma, J. C. Liu, H. Xiao and J. Li, *J. Am. Chem. Soc.*, 2018, **140**, 46–49.
- S. Vajda and M. G. White, *ACS Catal.*, 2015, **5**, 7152–7176.



- 24 P. Kaghazchi and T. Jacob, *Phys. Rev. B: Condens. Matter Mater. Phys.*, 2011, **83**, 035417.
- 25 Y.-K. Jeong, Y. M. Lee, J. Yun, T. Mazur, M. Kim, Y. J. Kim, M. Dygas, S. H. Choi, K. S. Kim, O.-H. Kwon, S. M. Yoon and B. A. Grzybowski, *J. Am. Chem. Soc.*, 2017, **139**, 15088–15093.
- 26 A. S. Chaves, G. G. Rondina, M. J. Piotrowski, P. Tereshchuk and J. L. F. Da Silva, *J. Phys. Chem. A*, 2014, **118**, 10813–10821.
- 27 O. Miramontes, F. Bonafé, U. Santiago, E. Larios-Rodriguez, J. J. Velázquez-Salazar, M. M. Mariscal and M. J. Yacaman, *Phys. Chem. Chem. Phys.*, 2015, **17**, 7898–7906.
- 28 N. Isomura, X. Wu and Y. Watanabe, *J. Chem. Phys.*, 2009, **131**, 164707.
- 29 S. Bonanni, K. Ait-Mansour, W. Harbich and H. Brune, *J. Am. Chem. Soc.*, 2012, **134**, 3445–3450.
- 30 A. Álvarez-García, J. C. Luque-Ceballos, L. O. Paz-Borbón and I. L. Garzón, *Comput. Mater. Sci.*, 2022, **214**, 111697.
- 31 S. Huseyinova, J. Blanco, F. G. Requejo, J. M. Ramallo-López, M. C. Blanco, D. Buceta and M. A. López-Quintela, *J. Phys. Chem. C*, 2016, **120**, 15902–15908.
- 32 A. R. Puigdollers, P. Schlexer, S. Tosoni and G. Pacchioni, *ACS Catal.*, 2017, **7**, 6493–6513.
- 33 P. G. Moses, A. Janotti, C. Franchini, G. Kresse and C. G. Van De Walle, *J. Appl. Phys.*, 2016, **119**, 181503.
- 34 L. O. Paz-Borbón, A. López-Martínez, I. L. Garzón, A. Posada-Amarillas and H. Grönbeck, *Phys. Chem. Chem. Phys.*, 2017, **19**, 17845–17855.
- 35 H. F. Wen, H. Sang, Y. Sugawara and Y. J. Li, *Phys. Chem. Chem. Phys.*, 2020, **22**, 19795–19801.
- 36 H. Xu and S. Y. Tong, *Surf. Sci.*, 2013, **610**, 33–41.
- 37 L. M. Liu, P. Crawford and P. Hu, *Prog. Surf. Sci.*, 2009, **84**, 155–176.
- 38 R. Y. Wang, J. X. Wang, J. Jia and H. S. Wu, *Appl. Surf. Sci.*, 2021, **536**, 147793.
- 39 C. Franchini, M. Reticcioli, M. Setvin and U. Diebold, *Nat. Rev. Mater.*, 2021, **6**, 560–586.
- 40 J. R. D. Lile, A. Bahadoran, S. Zhou and J. Zhang, *Adv. Theory Simul.*, 2022, **5**, 2100244.
- 41 M. Pilar de Lara-Castells, A. W. Hauser, J. M. Ramallo-López, D. Buceta, L. J. Giovanetti, M. A. López-Quintela and F. G. Requejo, *J. Mater. Chem. A*, 2019, **7**, 7489–7500.
- 42 P. López-Caballero, S. Miret-Artés, A. O. Mitrushchenkov and M. P. De Lara-Castells, *J. Chem. Phys.*, 2020, **153**, 164702.
- 43 P. López-Caballero, J. M. Ramallo-López, L. J. Giovanetti, D. Buceta, S. Miret-Artés, M. A. López-Quintela, F. G. Requejo and M. P. D. Lara-Castells, *J. Mater. Chem. A*, 2020, **8**, 6842–6853.
- 44 F. R. Negreiros, E. Aprà, G. Barcaro, L. Sementa, S. Vajda and A. Fortunelli, *Nanoscale*, 2012, **4**, 1208–1219.
- 45 L. O. Paz-Borbón, F. Buendía, I. L. Garzón, A. Posada-Amarillas, F. Illas and J. Li, *Phys. Chem. Chem. Phys.*, 2019, **21**, 15286–15296.
- 46 C. J. Heard, S. Heiles, S. Vajda and R. L. Johnston, *Nanoscale*, 2014, **6**, 11777–11788.
- 47 G. Kresse and J. Furthmüller, *Phys. Rev. B: Condens. Matter Mater. Phys.*, 1996, **54**, 11169–11186.
- 48 J. P. Perdew, K. Burke and M. Ernzerhof, *Phys. Rev. Lett.*, 1996, **77**, 3865–3868.
- 49 G. Kresse and D. Joubert, *Phys. Rev. B: Condens. Matter Mater. Phys.*, 1999, **59**, 1758–1775.
- 50 P. E. Blöchl, *Phys. Rev. B: Condens. Matter Mater. Phys.*, 1994, **50**, 17953–17979.
- 51 S. L. Dudarev, G. A. Botton, S. Y. Savrasov, C. J. Humphreys and A. P. Sutton, *Phys. Rev. B: Condens. Matter Mater. Phys.*, 1998, **57**, 1505–1509.
- 52 V. Ç. Çelik, H. Ünal, E. Mete and Ş. Ellialtıoğlu, *Phys. Rev. B: Condens. Matter Mater. Phys.*, 2010, **82**, 205113.
- 53 L. E. Gálvez-González, J. O. Juárez-Sánchez, R. Pacheco-Contreras, I. L. Garzón, L. O. Paz-Borbón and A. Posada-Amarillas, *Phys. Chem. Chem. Phys.*, 2018, **20**, 17071–17080.
- 54 E. Davari and D. G. Ivey, *Sustainable Energy Fuels*, 2018, **2**, 39–67.
- 55 E. Fernández, M. Boronat and A. Corma, *J. Phys. Chem. C*, 2015, **119**, 19832–19846.
- 56 M. Yu and D. R. Trinkle, *J. Chem. Phys.*, 2011, **134**, 064111.
- 57 W. Tang, E. Sanville and G. Henkelman, *J. Phys.: Condens. Matter*, 2009, **21**, 084204.
- 58 V. Wang, N. Xu, J.-C. Liu, G. Tang and W.-T. Geng, *Comput. Phys. Commun.*, 2021, **267**, 108033.
- 59 G. Henkelman, B. P. Uberuaga and H. Jónsson, *J. Chem. Phys.*, 2000, **113**, 9901–9904.
- 60 H. E. Saucedo, F. Salazar, L. A. Pérez and I. L. Garzón, *J. Phys. Chem. C*, 2013, **117**, 25160–25168.
- 61 A. Posada-Amarillas and I. L. Garzón, *Phys. Rev. B: Condens. Matter Mater. Phys.*, 1996, **54**, 10362.
- 62 J. Zhang and A. N. Alexandrova, *J. Phys. Chem. Lett.*, 2013, **4**, 2250–2255.
- 63 S. V. Ong and S. N. Khanna, *J. Phys. Chem. C*, 2012, **116**, 3105–3111.
- 64 D. E. Jiang, S. H. Overbury and S. Dai, *J. Phys. Chem. C*, 2012, **116**, 21880–21885.
- 65 Y. Wang and H. Gao, *J. Phys. Chem. B*, 2017, **121**, 2132–2141.
- 66 A. Álvarez-García, J. C. Luque-Ceballos, L. O. Paz-Borbón and I. L. Garzón, *Surf. Sci.*, 2023, **733**, 122287.
- 67 P. M. Kowalski, M. F. Camellone, N. N. Nair, B. Meyer and D. Marx, *Phys. Rev. Lett.*, 2010, **105**, 5–8.
- 68 T. Shibuya, K. Yasuoka, S. Mirbt and B. Sanyal, *J. Phys.: Condens. Matter*, 2012, **24**, 435504.
- 69 Q. Wu, S. Hou, D. Buceta, H. J. Ordoñez, M. Arturo López-Quintela and C. J. Lambert, *Appl. Surf. Sci.*, 2022, **594**, 153455.
- 70 G. Herzberg, *Molecular Spectra and Molecular Structure I: Spectra of Diatomic Molecules*, D. Van Nostran Company, 2nd edn, 1963, pp. 1–658.
- 71 R. Wang, L. Zhao, J. Jia and H. S. Wu, *AIP Adv.*, 2018, **8**, 035307.
- 72 M. Boronat, A. Pulido, P. Concepción and A. Corma, *Phys. Chem. Chem. Phys.*, 2014, **16**, 26600–26612.
- 73 P. P. Mkhonto, H. R. Chauke and P. E. Ngoepe, *Minerals*, 2015, **5**, 665–678.
- 74 M. Alducin, D. Sánchez-Portal, A. Arnau and N. Lorente, *Phys. Rev. Lett.*, 2010, **104**, 1–4.
- 75 Z. Dohnálek, J. Kim, O. Bondarchuk, J. M. White and B. D. Kay, *J. Phys. Chem. B*, 2006, **110**, 6229–6235.



- 76 I. Sokolovic, M. Reticcioli, M. Calkovsky, M. Wagner, M. Schmid, C. Franchini, U. Diebold and M. Setvín, *Proc. Natl. Acad. Sci. U. S. A.*, 2020, **117**, 14827–14837.
- 77 L. M. Molina and B. Hammer, *Phys. Rev. B: Condens. Matter Mater. Phys.*, 2004, **69**, 1–22.
- 78 L. B. Vilhelmsen and B. Hammer, *ACS Catal.*, 2014, **4**, 1626–1631.
- 79 Z. Duan and G. Henkelman, *Phys. Chem. Chem. Phys.*, 2016, **18**, 5486–5490.
- 80 J. Fabila, D. Romero, L. O. Paz-Borbón and F. Buendía, *J. Chem. Phys.*, 2022, **157**, 084309.

